Free locomotion of a flexible plate near the ground

Chengyao Zhang, Haibo Huang, and Xi-Yun Lu

Citation: Physics of Fluids **29**, 041903 (2017); doi: 10.1063/1.4981778
View online: http://dx.doi.org/10.1063/1.4981778
View Table of Contents: http://aip.scitation.org/toc/phf/29/4
Published by the American Institute of Physics

Free locomotion of a flexible plate near the ground

Chengyao Zhang, Haibo Huang,[a)] and Xi-Yun Lu
Department of Modern Mechanics, University of Science and Technology of China, Hefei 230026, China

(Received 4 December 2016; accepted 6 April 2017; published online 25 April 2017)

The free locomotion of a two-dimensional flapping flexible plate near the flat ground is studied by the lattice Boltzmann method for fluid flow and a finite-element method for the plate motion. The fluid flow and plate deformation are coupled through the immersed boundary scheme. When the leading edge of the plate is forced to oscillate sinusoidally near the ground, the plate may move freely in the horizontal direction due to the fluid-structure interaction. The mechanisms underlying the ground effect are elucidated. Besides a moderate rigidity, it is found that an appropriate density ratio between the plate and surrounding fluid (M) can improve the propulsive efficiency of the plate. When M is relatively small, the lateral force is enhanced, and the input work is increased when the plate is near the ground; when M is large, the deformation of the plate is inhibited and the input work is decreased when the plate is close to the ground. Usually the closer the plate flapping is to the wall, the more efficient the propulsion is, provided that the tail of the plate would not touch the wall. On the other hand, when the plate is close enough (within a critical lowest distance), the efficiency reaches a plateau with the highest efficiency. The vortices pattern and pressure field are also analyzed to explore the mechanism. This study may shed some light on mechanism for self-propulsion of a flexible plate near the ground. *Published by AIP Publishing.* [http://dx.doi.org/10.1063/1.4981778]

I. INTRODUCTION

When an aircraft or an animal flies or swims closely above a flat ground, aerodynamic or hydrodynamic benefits may be achieved due to the "ground effect."[1–3] The effect may include reducing induced drag and increasing lift. For example, a demersal teleost requires less power when hovering above the substrate,[1] a steelhead trout can reduce the expenditure of energy when swimming near the wall.[2] However, the mechanisms of such an unsteady ground effect remain still unclear,[4,5] and they are notable topics due to their biological and engineering applications.

In recent years, studies about free locomotion of a rigid foil have been performed.[6,7] In these studies, the rigid foil is actuated by heaving and pitching oscillations, which may result in a freely horizontal locomotion due to the interaction between the foil and surrounding fluid. On the other hand, a rigid plate model oscillating near the ground has been employed to understand the ground effect. For example, the ground effect on an elliptic foil hovering was studied numerically.[8] It is also investigated experimentally.[9] The ground effect on the flight of a bird is studied numerically with a rigid three-dimensional foil model.[10] A flapping foil towed at a constant propulsive speed oscillating near a solid wall is investigated experimentally.[11] Moreover, a rigid aerofoil undergoing pitching in the ground effect is studied experimentally and numerically,[12] and the result shows that the thrust can be enhanced by almost 40% in the ground effect.

On the other hand, the insect wings are usually flexible and they do not have an internal actuation mechanism; thus, the wings have to be passively deformed by the inertial-elastic or the fluid-dynamic force during flight.[13] If the leading edge of a flexible foil is actuated by heaving oscillations, or pitching oscillations, or both, the plate will end up developing deformations in the foil. Then the foil may move forward or "self-propelled"[14,15] due to the fluid-structure interaction. A self-propelled flexible foil undulating near a wall is studied experimentally.[16] In the study, the self-propulsion of the foil along a rectilinear trajectory was actuated by pitching oscillations at the leading-edge. The experimental data show that the wall can enhance the speed and thrust. The hydrodynamic benefits in the ground effect for a flexible panel have been investigated experimentally by Quinn *et al.*,[4] in which the panel is actuated by heaving oscillations at the leading-edge without pitching. The panels with three different bending stiffnesses were used. The study shows that the ground effect can increase the thrust and propulsive efficiency as the result of that the ground can suppress three-dimensional modes. The similar research topic was also studied numerically.[5] The study shows that the propulsion of the plate with a suitable degree of flexibility can be improved near the ground. Recently, Ryu *et al.*[17] numerically investigated a flexible flag heaving near the ground in a Poiseuille flow. It mainly focused on the effect of heaving frequency. In the study, only two different flapping amplitudes were investigated and the mass ratio was fixed. Dai *et al.*[18] also investigated the self-propelled swimming of a flexible plunging foil near the ground with a small flapping amplitude. In the study, effects of bending rigidity and gap distance are explored.

However, in the above self-propulsion studies, the inertial effect of the plate may play a critical role. The issue was usually ignored or was paid less attention. There are some studies on the inertial effect on other flapping problems instead of the self-propulsion problem. For example, the contributions of the inertial-elastic and aerodynamic forces to the bending

[a)]Author to whom correspondence should be addressed. Electronic mail: huanghb@ustc.edu.cn

of the wing in the hawkmoth *Manduca sexta* have been examined by an experimental approach.[19] In the test, the wing flaps around the wing hinge with a sinusoidal motion. The inertial effect of the wing on hovering flight has been performed.[20,21] Hence, to the best of our knowledge, the inertial effect on the self-propulsive performance of the plate near a wall has never been carried out.

In this study, the self-propulsion of a flapping flexible plate is used to mimic the swimming of a fish near the ground. The plate is forced to oscillate sinusoidally at the leading-edge near a solid ground in a stationary fluid, which is similar to those in Refs. 4 and 5. The effect of density ratio between the plate and surrounding fluid (M) is investigated in detail. The ground effect on the propulsive speed, propulsive efficiency, the vortical structure and pressure distribution around the plate, and the deformation of the plate is studied.

This paper is organized as follows: The physical problem and mathematical formulation are presented in Sec. II. The numerical method and validation are described in Sec. III. Results are discussed in Sec. IV and concluding remarks are addressed in Sec. V.

II. PHYSICAL PROBLEM AND MATHEMATICAL FORMULATION

As shown in Figure 1, we consider a flexible plate with length L which is placed in proximity to a planar ground. The surrounding fluid is stationary. The leading-edge of the plate is forced to perform a vertical oscillation described as

$$y(t) = A_0 \cos(2\pi f t), \tag{1}$$

where A_0 and f are the oscillating amplitude and frequency, respectively. The average distance between the leading-edge of the plate and the ground is d. Here, a Lagrangian coordinate s along the plate surface is defined to describe the configuration and motion of the plate.

Due to the interplay of the plate elasticity, the leading-edge forcing, and the forces exerted by the surrounding fluid, the plate starts to move freely and passively in the stationary fluid. The active pitching angle is zero in this model; it means that only the leading-edge of the plate is restricted with a prescribed vertical motion and the remainder of the plate can move freely in the entire fluid domain.

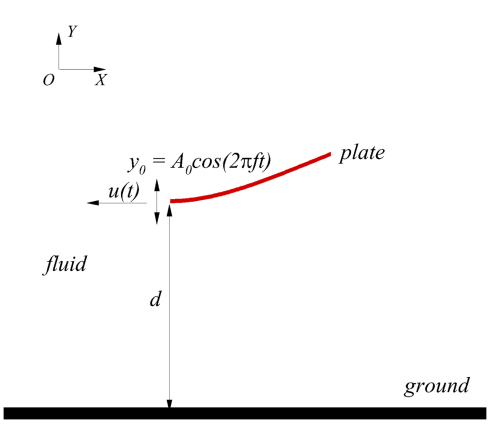

FIG. 1. Schematic of a flapping flexible plate near the ground.

To investigate this system of the fluid and flapping flexible plate interaction, the incompressible Navier-Stokes equations are solved to simulate the fluid flow,

$$\frac{\partial \boldsymbol{v}}{\partial t} + \boldsymbol{v} \cdot \nabla \boldsymbol{v} = -\frac{1}{\rho}\nabla p + \frac{\mu}{\rho}\nabla^2 \boldsymbol{v} + \boldsymbol{f}, \tag{2}$$

$$\nabla \cdot \boldsymbol{v} = 0, \tag{3}$$

where $\boldsymbol{v}$ is the velocity, p the pressure, ρ the density of the fluid, μ the dynamic viscosity, and $\boldsymbol{f}$ the body force term.

The structural equation is employed to describe the plate deformation and motion,[22–24]

$$\rho_s h \frac{\partial^2 \boldsymbol{X}}{\partial t^2} - Eh\frac{\partial}{\partial s}\left[\left(1 - \left(\frac{\partial \boldsymbol{X}}{\partial s}\cdot\frac{\partial \boldsymbol{X}}{\partial s}\right)^{-1/2}\right)\frac{\partial \boldsymbol{X}}{\partial s}\right] + EI\frac{\partial^4 \boldsymbol{X}}{\partial s^4} = \boldsymbol{F}_s, \tag{4}$$

where s is the Lagrangian coordinate along the plate, $\boldsymbol{X} = (X, Y)$ is the position vector of the plate, $\boldsymbol{F}_s$ is the Lagrangian force exerted on the plate by the fluid, and $\rho_s h$ is the structural linear mass density of the plate. Eh and EI are the stretching and the bending stiffnesses of the plate, respectively.

For the plate, the following boundary conditions:

$$y(t) = A_0 \cos(2\pi f t), \frac{\partial \boldsymbol{X}}{\partial s} = (1, 0), \tag{5}$$

and

$$\left(\frac{\partial \boldsymbol{X}}{\partial s}\cdot\frac{\partial \boldsymbol{X}}{\partial s}\right)^{-1/2} = 1, \quad \frac{\partial^3 \boldsymbol{X}}{\partial s^3} = 0, \quad \frac{\partial^2 \boldsymbol{X}}{\partial^2 s} = 0, \tag{6}$$

are imposed at the leading-edge and the trailing-edge, respectively.

The characteristic quantities ρ, L, and f are chosen to normalize the above equations and key parameters. Here ρ is the fluid density, L the length of the plate, and f the heaving frequency. The characteristic speed is defined as $U_{ref} = Lf$, the characteristic time $T_{ref} = L/U_{ref}$, and the flapping period $T = 1/f$. The normalized governing parameters are described as follows: the heaving amplitude $A = A_0/L$, the Reynolds number $Re = \rho f L^2/\mu$, the stretching coefficient $S = Eh/\rho f^2 L^3$, the bending coefficient $K = EI/\rho f^2 L^5$, the mass ratio of the plate and the fluid $M = \rho_s h/\rho L$, and the ground distance between the mean location of leading-edge of plate and the ground $D = d/L$.

III. NUMERICAL METHOD AND VALIDATION

The fluid flow is solved by the lattice Boltzmann method[24,25] and the motion of the flexible plate is solved by the finite element method. The immersed boundary (IB) scheme is used to couple the two solvers.[26,27] In the IB scheme, the Lagrangian force $\boldsymbol{F}_s$ in Eq. (4) can be calculated by the penalty method,[24,28–30]

$$\boldsymbol{F}_s(s,t) = \alpha \int_0^t [\boldsymbol{V}_f(s,t') - \boldsymbol{V}_s(s,t')]\mathrm{d}t' + \beta[\boldsymbol{V}_f(s,t) - \boldsymbol{V}_s(s,t)], \tag{7}$$

where α and β are penalty parameters which are selected based on the previous studies,[8,15,31] $V_s = \frac{\partial \boldsymbol{X}}{\partial t}$ is the plate velocity and

V_f is the fluid velocity at the Lagrangian position $\boldsymbol{X}$, which is obtained by interpolation

$$\boldsymbol{V}_f(s,t) = \int \boldsymbol{v}(x,t)\delta(\boldsymbol{x} - \boldsymbol{X}(s,t)]\mathrm{d}\boldsymbol{x}. \tag{8}$$

In the IB scheme, the body force term $\boldsymbol{f}$ in Eq. (2) is used as an interaction force between the fluid and the immersed boundary to enforce the no-slip velocity boundary condition. The body force $\boldsymbol{f}$ on the Eulerian points can be obtained from the Lagrangian force $\boldsymbol{F}_s$ using the Dirac delta function, i.e.,

$$\boldsymbol{f}(x,t) = \int \boldsymbol{F}_s(s,t)\delta(\boldsymbol{x} - \boldsymbol{X}(s,t)]\mathrm{d}s. \tag{9}$$

Eq. (4) for the deformable plate is discretized by a finite element method, and the deformation with large-displacement of the plate is handled by the co-rotational scheme.[32] A detailed description of the numerical method can be found in our previous studies.[15,24]

The numerical strategy used here has been successfully applied to a wide range of flows, such as dynamics of an inverted flexible plate,[33] dynamics of fluid flow over a circular flexible plate,[24] locomotion of a flapping flexible plate,[15] and vorticity dynamics of fluid flow over flapping plate.[34] To further validate the numerical method, a flapping flag in a uniform flow[29] was simulated with parameters $Re = 200$, $M = 1.5$, $K = 0.001$, and $S = 1000$. Figure 2 shows the time history of the lateral displacement of the trailing-edge of the flag. It is seen that the displacement magnitude is consistent with that from Ref. 29 but with a small phase shift after it reaches a periodic state ($\frac{t}{T} > 20$).

Since in our study the length is normalized by L, the nondimensional length of the plate is unity. Moreover, a finite moving computational domain[15,35] is used in the x-direction to allow the plate to move in the x-direction for a sufficiently long time. As the plate travels one lattice in the x-direction, the computational domain is shifted, i.e., one layer being added at the inlet and another layer being removed at the outlet.[15,35]

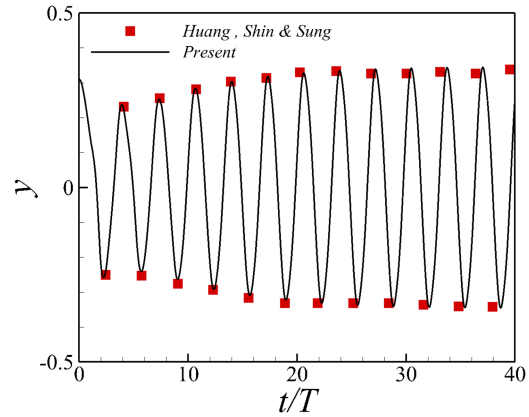

FIG. 2. The lateral displacement of the trailing-edge of a flag in a uniform flow as a function of time. The solid line and points represent the present result and that from Ref. 29, respectively.

For the grid independence study, cases with $\Delta x = 0.005$, 0.01, and 0.02 were tested and in the three cases $\Delta t = 0.0001$. In the time step independence study, cases with $\Delta t = 0.000\,05$, 0.0001, and 0.0002 were tested and in the three cases $\Delta x = 0.01$. The results for grid independence and time step independence studies are presented in the left and right columns of Figure 3. In the figure, the upper and lower rows represent the propulsive velocity of the flapping flexible plate U and the vorticity at point (−4.5, −3.9) as a function of time, respectively.

For the grid independence study, Figure 3(a) shows that the velocity curves for $\Delta x = 0.01$ and $\Delta x = 0.005$ are very close. Figure 3(c) shows that the vorticity curves for $\Delta x = 0.01$ and $\Delta x = 0.005$ also agree very well. On the other hand, the curve of $\Delta x = 0.02$ has significant discrepancies with those of $\Delta x = 0.01$.

For the time step independence study, from both Figures 3(b) and 3(d), it is seen that the curves for $\Delta t = 0.0001$ and $\Delta t = 0.000\,05$ agree very well but the curve for $\Delta t = 0.0002$ has significant discrepancies with them.

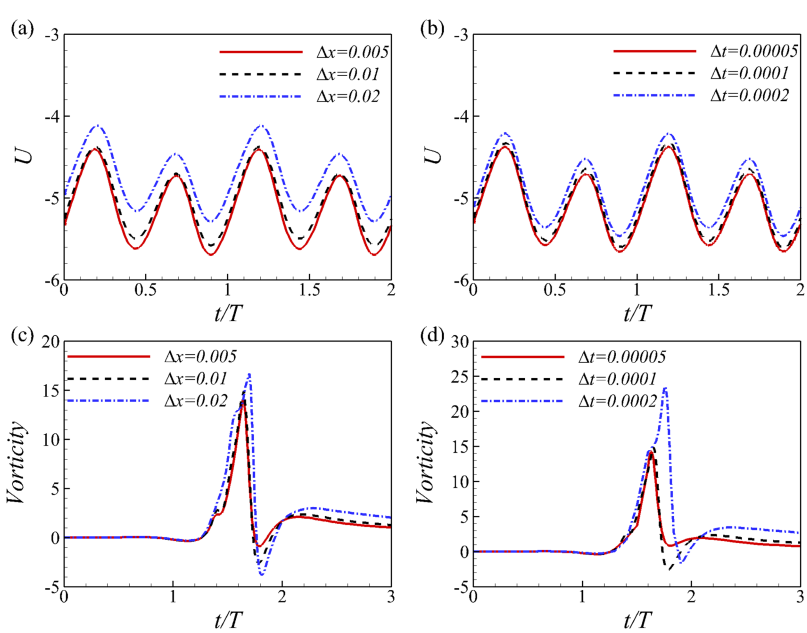

FIG. 3. The grid independence and time step independence studies for the case with $M = 0.2$, $A = 0.4$, $D = 0.6$, $K = 5$, $S = 1000$, and $Re = 100$. (a) and (b) are leading-edge's horizontal velocities as a function of time; (c) and (d) are vorticities at one mark point (−4.5, −3.9). The point is close to the ground which is located at $y = -4$. When the plate passes by, this mark point is also close to the lower surface of the plate.

Hence, the results of the convergence tests show that $\Delta x = 0.01$ and $\Delta t = 0.0001$ are small enough to obtain accurate results. In all of the following numerical simulations, the mesh space $\Delta x = 0.01$ and time step $\Delta t = 0.0001$ are adopted. In the simulations, the Dirichlet boundary condition $\boldsymbol{v} = 0$ is applied at the top and bottom boundaries, and the Neumann boundary condition $\frac{\partial \boldsymbol{v}}{\partial x} = 0$ is used at the inlet and the outlet. To minimize the effect of boundary condition, the nondimensional computational domain for the fluid flow is chosen as $[-5, 25] \times [-5, 10]$ in the x and y directions.

IV. RESULTS AND DISCUSSION

In our study, motivated by the investigation of the animal locomotion,[19,36–43] the Reynolds number is fixed to be $Re = 100$ and the plate is inextensible with a large stretching coefficient $S = 1000$. The bending coefficient is fixed to be $K = 5$. The other parameter ranges in this study are $D \in (0.3, 4.0)$, the heaving amplitude $A \in (0.1, 0.55)$, and the mass ratio $M \in (0.1, 1.5)$.

A. Propulsive performance in ground effect

The propulsive performance of the plate is shown in Figure 4. Figure 4(a) shows the normalized time-averaged propulsive speed U as a function of D. As D increases, the speed U decreases monotonously if $D \le 1.5$; when $D > 1.5$, the speed U is almost a constant. The ground effect increases the propulsive speed for all flapping amplitudes considered here.

The input work W as a function of D is shown in Figure 4(b). The input work W is required to maintain the self-propulsion of the flapping plate and computed as a time integral of the power P performed by the surface of the body on the surrounding fluid over one flapping period, i.e.,

$$W = \int_{t_0}^{t_0+T} P \mathrm{d}t = \int_{t_0}^{t_0+T} \int_0^1 \boldsymbol{F}_r(s,t) \cdot \frac{\partial \boldsymbol{X}(s,t)}{\partial t} \mathrm{d}s\mathrm{d}t, \quad (10)$$

where $\boldsymbol{F}_r$ represents the force on the surrounding fluid by the flapping plate. It is seen that the trend of W is similar to that of U. It is conjectured that the increase of the propulsive speed is at the expense of the rising input power.[18] This issue will be discussed below after Figure 5 is described.

To quantify the propulsive efficiency of the plate, the ratio of the kinetic energy of the body and the input work has been employed.[15,35,44] Therefore the propulsive efficiency is $\eta = \frac{1}{2} M U^2 / W$. The propulsive efficiency as a function of D is shown in Figure 4(c). It is seen that when D decreases from 1.5 to 0.5, the η increases rapidly, when $D > 1.5$ the propulsive efficiency is almost a constant. Hence, it seems that more input work was converted into the kinetic energy of the plate when the flapping motion is closer to the ground (smaller D).

Figure 4(d) shows the mean lift coefficients C_L as functions of D. The variations of C_L in all cases with different D have a similar trend. Here we take the result of the case $A = 0.4$ as a typical example to elucidate the propulsive behaviors. The variation has two distinct regimes. When $D \le 1.5$, C_L is positive and decreases with D, and it tends to push the plate away from the ground; when $D > 1.5$, C_L is negative and tends to pull the plate towards the ground, and it decreases with D first then increases and approaches to zero as $D \to \infty$. The C_L behavior is consistent with that of the unsteady propulsion of a pitching rigid foil near the ground.[4]

The effect of the density ratio M on propulsive behaviors is shown in Figure 5 for $M \in (0.1, 1.4)$. For cases with a larger M, due to large inertia of the plate, the inertial force instead of the fluid force (induced by pressure difference and viscous force) acting on the plate may have a major effect on its deformation and movement. Hence, $M > 1.4$ is not considered here. It is also noticed that for $D = 0.6$ and $D = 0.7$, when $M > 1.2$, the plate would touch the wall and the simulation is unable to be performed. Therefore, there are less data for cases with a smaller D in Figure 5.

Figure 5(a) shows the propulsive speed U as a function of M. For cases $D = 0.7$, 0.8, 1.0, and ∞, after the speed reaches a

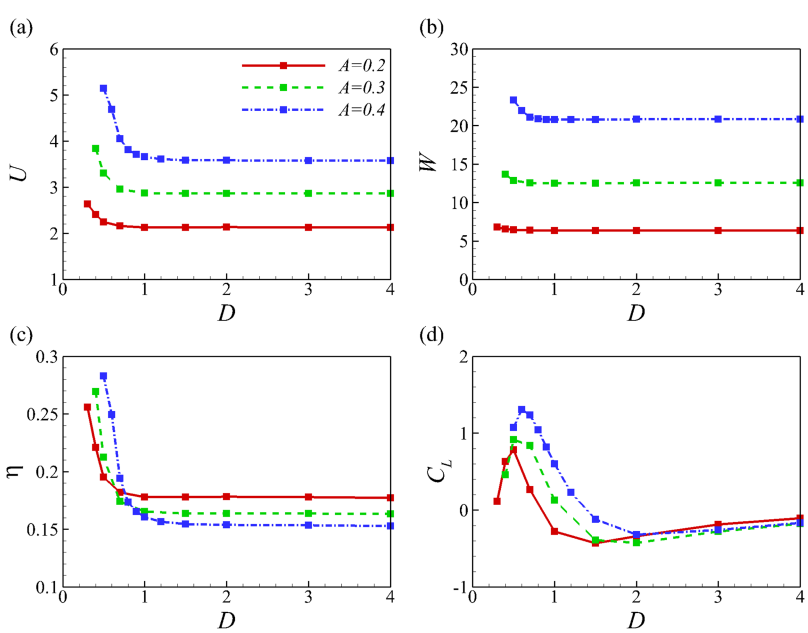

FIG. 4. (a) Propulsive speed, (b) input work in one flapping period, (c) propulsive efficiency, and (d) mean lift coefficient as functions of distance D for $M = 0.5$. The lines represent cases with $A = 0.2$, 0.3, and 0.4, respectively.

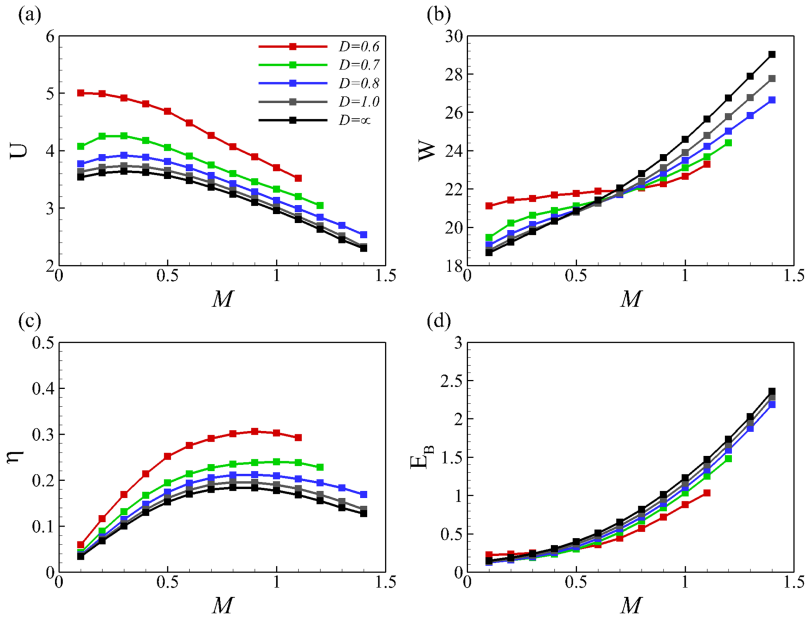

FIG. 5. (a) Mean propulsive speed, (b) input work in one flapping period, (c) propulsive efficiency, and (d) the bending energy as functions of density ratio M with $A = 0.4$.

maximum at $M \approx 0.3$, it decreases with the increasing M. For the cases with $D = 0.6$, U decreases monotonically. Figure 5(b) shows that the input work W increases monotonically with M. For the propulsive efficiency (see Figure 5(c)), the maximum propulsive efficiency occurs approximately at $M = 0.8$ for cases with all distances.

Although U decreases with M, the kinetic energy of the plate $\frac{1}{2}MU^2$ generally increases with M. The increase of the kinetic energy and the input work is convex (not shown here) and concave (see Figure 5(b)), respectively. Hence, the propulsive efficiency $\eta = \frac{\frac{1}{2}MU^2}{W}$ as a function of M is convex and the highest efficiencies are achieved at a moderate density ratio ($M \approx 0.8$). Figures 5(a) and 5(b) also show that at a larger M, e.g., $M = 1.0$, W decreases but U increases as the flapping is closer to the wall. Hence, the conjecture that the increase of U is at the expense of the rising input power[18] seems not correct for cases with a larger M.

Figure 5(b) also shows that for a smaller M, the input work W increases as the plate is flapping closer to the wall (at a smaller D). The situation is reversed for a relatively larger M, e.g., $M = 1.2$.

As the plate is flexible, it can store elastic potential energy because of the fluid-plate interaction. It is noted that the elastic potential due to the stretching effect is negligible due to the large S. Thus the elastic potential energy is defined as

$$E_B(t) = \frac{K}{2}\int_0^L \frac{\partial^2 \boldsymbol{X}}{\partial s^2}\cdot\frac{\partial^2 \boldsymbol{X}}{\partial s^2}\mathrm{d}s, \tag{11}$$

where K is the normalized bending stiffness defined as $K = EI/\rho f^2 c^5$. Figure 5(d) shows the bending energy of the plate increases monotonically with M, which may be due to the inertial effect. Since the locomotion velocity U decreases with increasing M (see Figure 5(a)), it seems that larger deformation of the plate for large density ratio causes negative effect on the locomotion.

The effect of the density ratio M on propulsive behaviors is shown in Figure 6 for $A = 0.1$. Figure 5(a) shows that U increases to a peak at $M \approx 0.7$, then decreases with increasing M. Figure 5(b) shows the input work W also increases first and then decreases. For the propulsive efficiency (Figure 5(c)), η increases monotonically with M for $D = 0.3$, but for other Ds, the maximum ηs are achieved at $M \approx 1.2$.

From Figures 5(a), 5(b), 6(a), and 6(b), it is also seen that the conjecture that the increase of U is at the expense of the rising input power[18] seems only valid for a smaller M. For a larger M, it is not valid. The possible mechanism will be explored in Secs. IV B and IV C.

Then we would like to directly compare the propulsive performances between the near-ground case and the corresponding cases without the ground and isolate the role of the ground. Here the influence of flapping amplitude A on propulsive performance of the plate is shown in Figure 7. From Figure 7(a), it is seen that U increases monotonically with A for both cases with and without the ground. The net increment of U due to the ground effect (i.e., ΔU) increases with A and reaches to its maximum at $A = 0.45$, then goes down. Figure 7(b) shows that the input works in cases $D = 0.7$ and $D = \infty$ are almost identical when $A < 0.45$. When $A > 0.45$, the increment of W is also negligible with the maximum increment approximately 5% at $A = 0.55$.

We would like to demonstrate that there is benefit from the ground effect. Because ΔU increases fast when $A \in (0.3, 0.45)$ and ΔW is almost zero in the region, $\Delta\eta$ increases in the region and approaches its maximum at $A = 0.45$, which is shown in Figure 7(c). That means at $A \in (0.3, 0.45)$, the ground effect significantly enhances the propulsive efficiency in the near-ground cases, which is referred to as the "benefit-increase" regime. When $A > 0.45$, the ground effect on the enhancement of efficiency $\Delta\eta$ decreases and it is referred to as the "benefit-decrease" regime. It is noticed that in the "benefit-decrease" regime, the propulsive efficiency reaches a plateau with highest efficiency.

From Figure 7(d), it is seen that for the bending energy E_B, the ground effect can also be classified into two regimes,

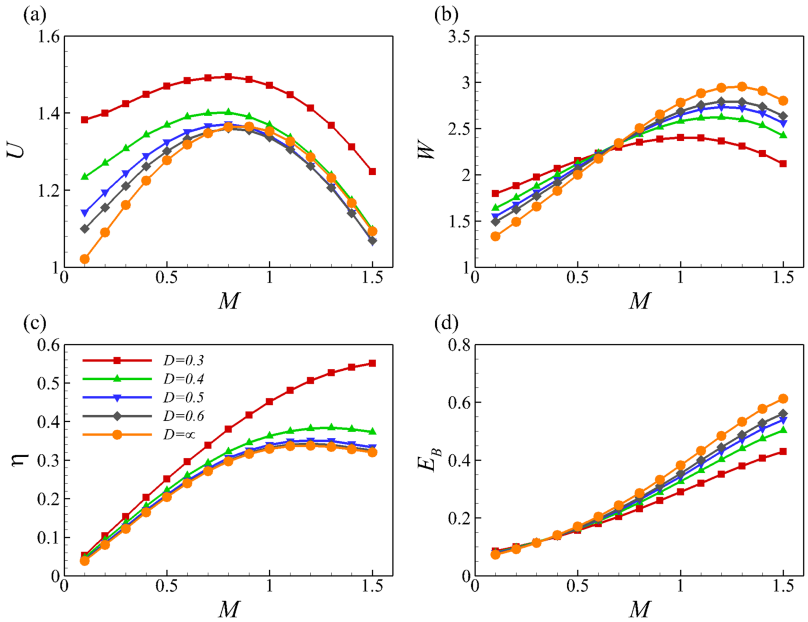

FIG. 6. (a) Mean propulsive speed, (b) input work in one flapping period, (c) propulsive efficiency, and (d) the bending energy as functions of density ratio M with $A = 0.1$.

$A < 0.45$ and $A > 0.45$. Here $A = 0.45$ is a critical value. When $A < 0.45$, the ground inhibits the deformation of the plate because $\Delta E_B < 0$, and the inhibition increases with A as $A \leq 0.4$; when $A > 0.45$, the ground enhances the deformation of the plate ($\Delta E_B > 0$). It is noted that a larger oscillation amplitude requires more vertical space (a larger D) for flapping freely otherwise the tail of the plate may touch the ground. For example, in the case $D = 0.7$, the largest flapping amplitude allowed is about $A = 0.55$.

In summary, the propulsion of the plate is able to benefit from the ground effect. However, for a specific distance D, two distinct regimes which are separated by a critical flapping amplitude A_{cr} are identified, i.e., "benefit-increase" and "benefit-decrease" regimes. In the two regimes, the deformation of the plate is enhanced and inhibited, respectively. When $A > A_{cr}$, the propulsive efficiency reaches a plateau with highest efficiency.

B. Unsteady dynamics and deformation of plate

In order to understand the propulsive behaviors in the ground effect, unsteady dynamics and deformation of the plate are further investigated. Figure 8 shows drag coefficients and input powers as functions of time in one flapping period. Here the flapping amplitude A is fixed to be 0.4 to investigate the effect of D. Figure 8(a) shows C_D curves for a relatively smaller M ($M = 0.3$) and the curves of C_D for cases with different D are essentially similar. The minor difference is that the maximum thrust, i.e., the magnitude of the negative drag increases as D decreases. The input power P as a function of time is shown in Figure 8(b). For the cases with a smaller D, e.g., $D = 0.5$ (the solid red line), P increases in most period of one flapping cycle compared to the case with a larger D. Hence, the input work increases if the flapping is closer to the ground (smaller D), which is consistent with the result in Figure 5(b) for $M = 0.3$.

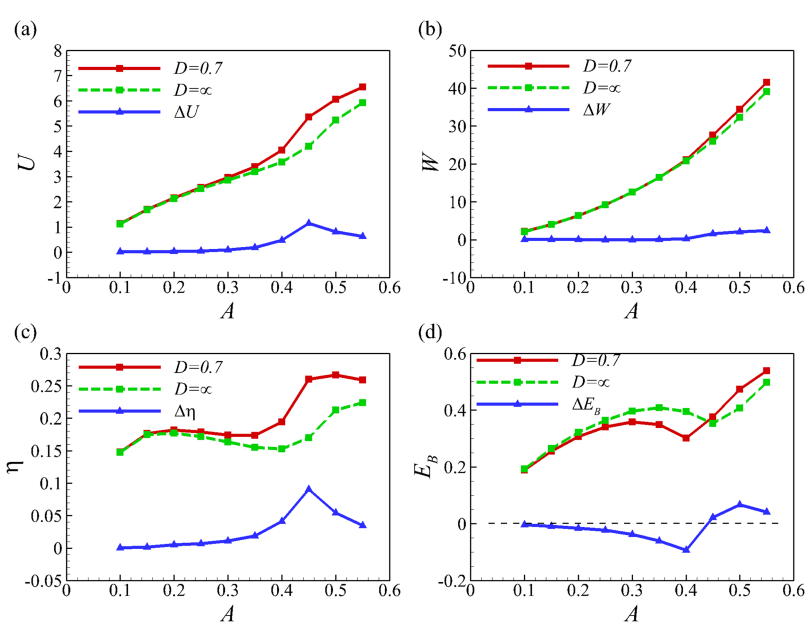

FIG. 7. The influence of flapping amplitude A on the propulsive metrics: (a) mean propulsive speed U, (b) input work in one flapping period W, (c) propulsive efficiency η, and (d) bending energy E_B with $M = 0.5$. Δ means the value of $D = 0.7$ case minus that in the case of $D = \infty$. The dashed line in (d) presents $\Delta E_B = 0$.

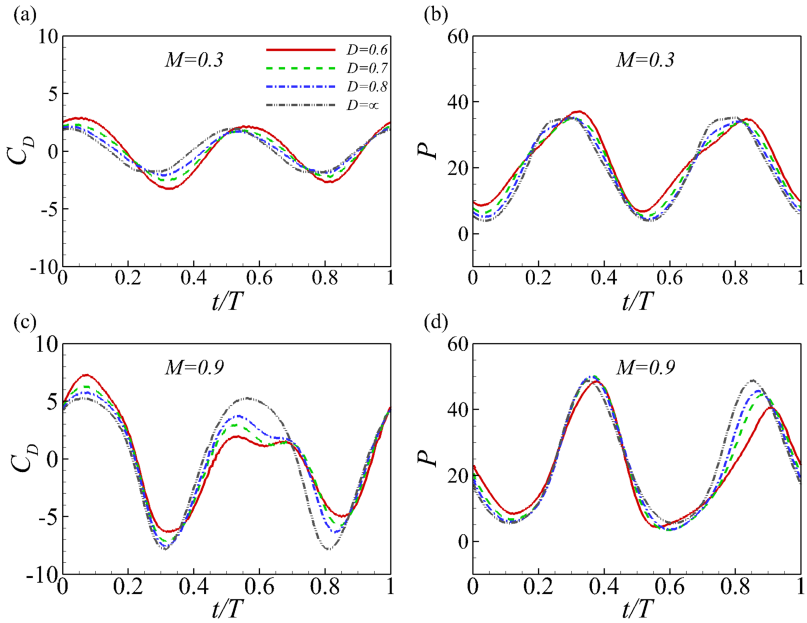

FIG. 8. (a) Drag coefficient C_D and (b) input power P as functions of time in one flapping cycle for $M = 0.3$ with $A = 0.4$, (c) drag coefficient C_D and (d) input power P as functions of time in one flapping cycle for $M = 0.9$ with $A = 0.4$.

For cases with a larger M, e.g., $M = 0.9$, the curves of C_D for cases with different D are shown in Figure 8(c). Figure 8(c) looks similar to Figure 8(a). A minor difference is that the thrust or negative drag increases with D, which is different from that in Figure 8(a). Compared to Figure 8(a), the amplitude of the drag coefficient is much larger in Figure 8(c) for each D. Hence, the thrust force magnitude in the case with $M = 0.9$ is larger than that in the corresponding case for $M = 0.3$.

Figure 8(d) shows that the input power increases with D especially in the period $0.7 < t/T < 0.9$; thus, the total input work W in one period slightly increases with D for $M = 0.9$, which is consistent with that in Figure 5(b) for $M = 0.9$.

Then we would like to discuss the ground effect on the deformation of the plate. The plate deformation shapes at eight instances during one flapping cycle for four cases (see Table I) are shown in Figure 9. For $M = 0.3$, compared with Case 1B, the deformation in Case 1A is enhanced at all instances except $t/T = 0$, 0.125, and 0.625. It seems that the presence of the ground also significantly modifies the phase of the plate deformation. Hence, the vertical trailing edge displacement relative to the leading edge during a steady period for $M = 0.3$ is also plotted in Figure 9(c). It is seen that overall, except for the phase of plate deformation, the deformation is not sensitive to the distance for $M = 0.3$, which is consistent with that in Figure 5(d). However, for $M = 0.9$, Figure 9(b) shows that the plate deformation is overall inhibited except at $t/T = 0.875$. Figure 9(d) also confirmed that the flapping is inhibited due to the presence of ground. It is also seen that without the ground, due to the inertial effect of the plate, the deformation at a larger M (black lines in Figure 9(b)) is more significant than that at a smaller M (black lines in Figure 9(a)).

TABLE I. Parameters for four specified cases.

Case	M	D	A
Case 1A	0.3	0.6	0.4
Case 1B	0.3	∞	0.4
Case 2A	0.9	0.6	0.4
Case 2B	0.9	∞	0.4

The drag coefficient and input power as functions of time in one flapping cycle for $A = 0.1$, 0.4, 0.45, and 0.5 are shown in Figure 10. The ground effect on C_D is shown in Figure 10(a). It is noted that the integration of C_D is zero for all cases due to the horizontal free locomotion of the plate. When the flapping amplitude A is small, e.g., $A = 0.1$, the ground effect on C_D is negligible. It is also seen that when A is larger, the C_D variation magnitude in the case of $D = 0.7$ is larger than that in the corresponding case of $D = \infty$. That means a larger thrust and a drag are generated during the downstroke and upstroke periods, respectively, when the flapping is close to the wall.

Figure 10(b) shows that the input power P as a function of time in one flapping cycle. When the flapping amplitude A is small, e.g., $A = 0.1$, the ground effect on P is negligible. For a larger amplitude, e.g., $A = 0.5$, during most period of the cycle, the power P of the case with $D = 0.7$ is larger than that in the corresponding case with $D = \infty$. That means more input work is required due to the ground effect. On the other hand, during most period of the cycle, the power P increases with A for $D = 0.7$ and $D = \infty$, respectively. Hence, the overall input work (integration of input power) increases with A for cases of $D = 0.7$, so do the cases of $D = \infty$. All these dynamic behaviors are consistent with the results in Figure 7(b).

For cases with $A = 0.4$ and 0.5, Figures 11(a) and 11(b) show the instantaneous shapes of the plate. It is seen that compared to the corresponding case without the ground, the deformation is inhibited overall in the whole flapping cycle for $A = 0.4$ (left column) but enhanced for $A = 0.5$ (right column). Figures 11(c) and 11(d) also confirmed this point. It is consistent with the results shown in Figure 7(d). It is noticed that the deformation is still inhibited when the plate is

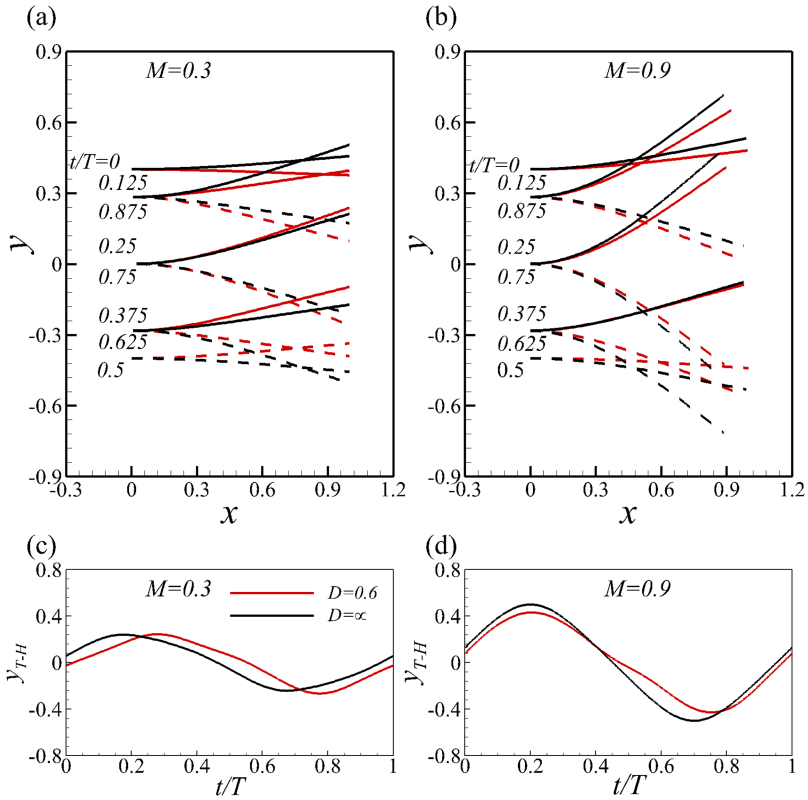

FIG. 9. Plate deformation shapes at eight instances during one flapping cycle for four cases (see Table I) with (a) $M = 0.3$ and (b) $M = 0.9$. The red lines and black lines represent the shapes at $D = 0.6$ and $D = \infty$, respectively. The solid and dashed lines represent the downstroke and the upstroke periods, respectively. The vertical trailing edge displacement relative to the leading edge during a steady period for (c) $M = 0.3$ and (d) $M = 0.9$.

very close to the wall (e.g., $t/T = 0.625$) despite the overall enhancement in the whole flapping cycle.

C. Vortical structure and pressure distribution

The propulsive behaviors of the flapping flexible plate are closely associated with the vortical structures; thus, we further discuss the vortical structures around the plate and the pressure distribution on the plate.

Figure 12 shows the vorticity contours at four instants of one flapping cycle for Case 1A and Case 1B (Table I). Without the ground effect, the reverse Karman vortex street is seen in the right column of Figure 12. The wake behind the flapping plate with the ground effect becomes complex (see the left column of Figure 12), and the vortical structures are no longer symmetric in the wake, resulting in lift generation.

To investigate the connection of the vortical structures and the forces on the plate, Figure 13 shows the pressure contours corresponding to the four instants in Figure 12. At $t/T = 0$, the pressure around the plate leading edge in Figure 13(a) is higher than that in Figure 13(e). Because the plate in Case 1A moves faster than Case 1B as shown in Figure 5(a), correspondingly it encounters a greater resistance.

During the downstroke period, at $t/T = 0.25$, the pressure between the plate and the ground increases in Figure 13(b) compared to Figure 13(f). Hence, a more significant lift force is generated in Case 1A than that in Case 1B. The deformation of the plate is also slightly larger in Figure 13(b).

As the leading-edge flaps to the nearest location away from the ground at $t/T = 0.5$, because of the ground effect, the pressure below the plate in Figure 13(c) is higher than that in Figure 13(g). At the time, the deformation in Case 1A is almost identical to 1B but it has a reverse deflection. When the plate flaps upwards at $t/T = 0.75$, the pressure in both the upper and lower surfaces is reduced in Figure 13(d), compared to that in Figure 13(h).

The vorticity contours for $M = 0.9$ (Case 2A and 2B) are shown in Figure 14. It is seen that the wake behind the plate for Case 2B, which is shown in the right column, is the reverse Karman vortex street. The vortices distances in Case 2A and 2B (Figure 14) are smaller than those in Case 1A and 1B

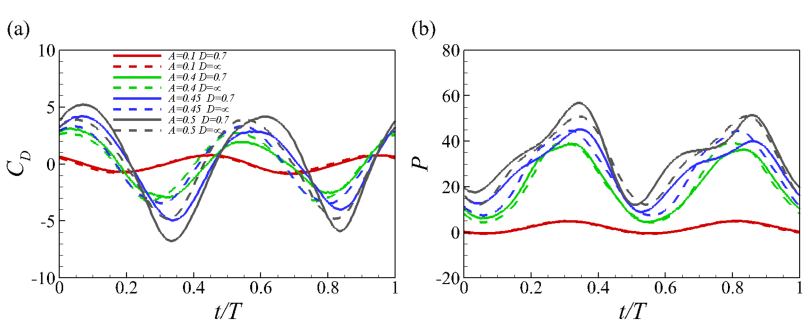

FIG. 10. Time-dependent (a) drag coefficient and (b) input power in one flapping cycle for $A = 0.1$, 0.4, 0.45, and 0.5 with $M = 0.5$.

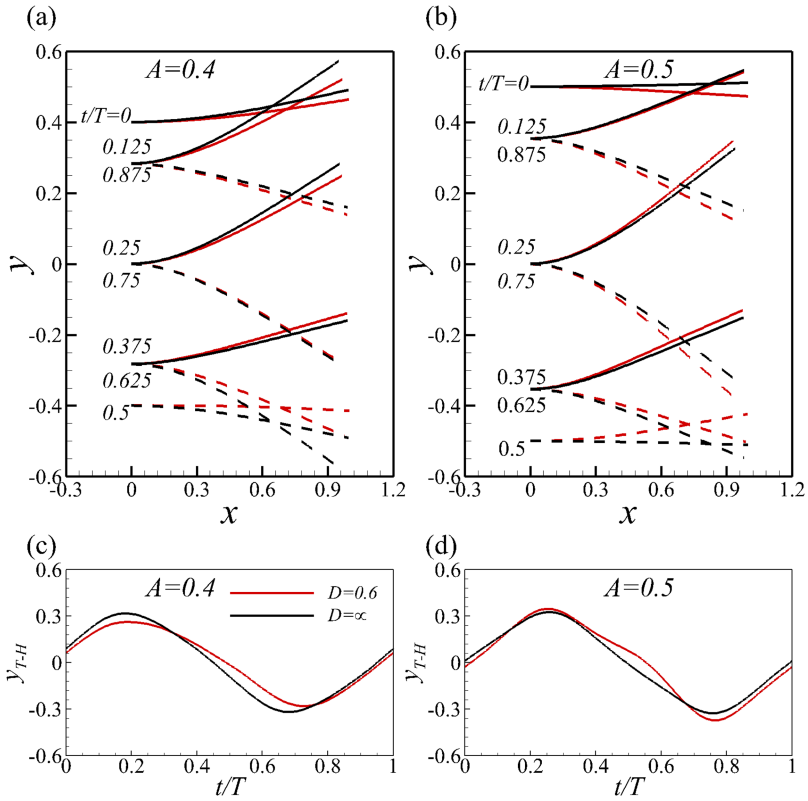

FIG. 11. Plate deformation shapes at eight instances during one flapping cycle with $M = 0.5$ for (a) $A = 0.4$ and (b) $A = 0.5$. The red and black lines represent the shapes at $D = 0.7$ and $D = \infty$, respectively. The solid and dashed lines represent the downstroke and upstroke periods, respectively. The vertical trailing edge displacement relative to the leading edge during a steady period for (c) $A = 0.4$ and (d) $A = 0.5$.

(Figure 12), respectively. That means the propulsive speed U in Case 2A and 2B is smaller than that in Cases 1A and 1B, respectively. This is consistent with the result in Figure 5(a).

The pressure contours at typical instants of one flapping cycle for Case 2A and 2B are shown in the left and right columns, respectively, in Figure 15. At $t/T = 0$, the pressure

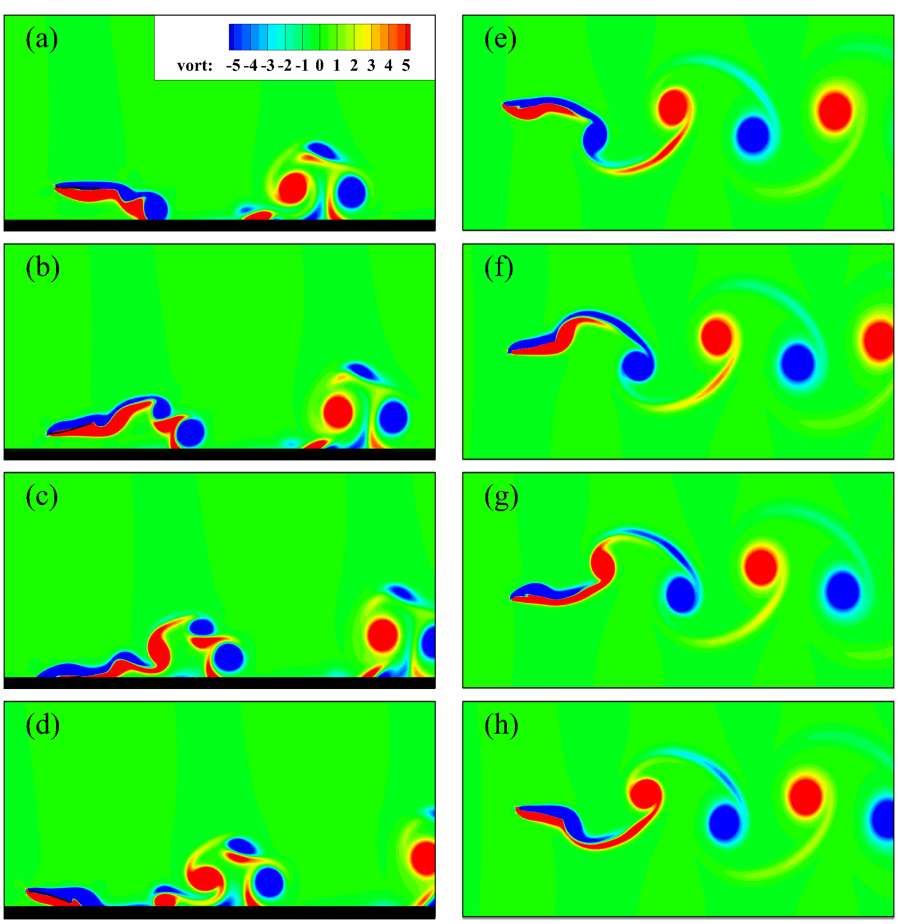

FIG. 12. Vorticity contours at typical instants of one flapping cycle for Case 1A (left column) and Case 1B (right column) with $M = 0.3$: ((a) and (e)) $t/T = 0$, ((b) and (f)) 0.25, ((c) and (g)) 0.5, and ((d) and (h)) 0.75.

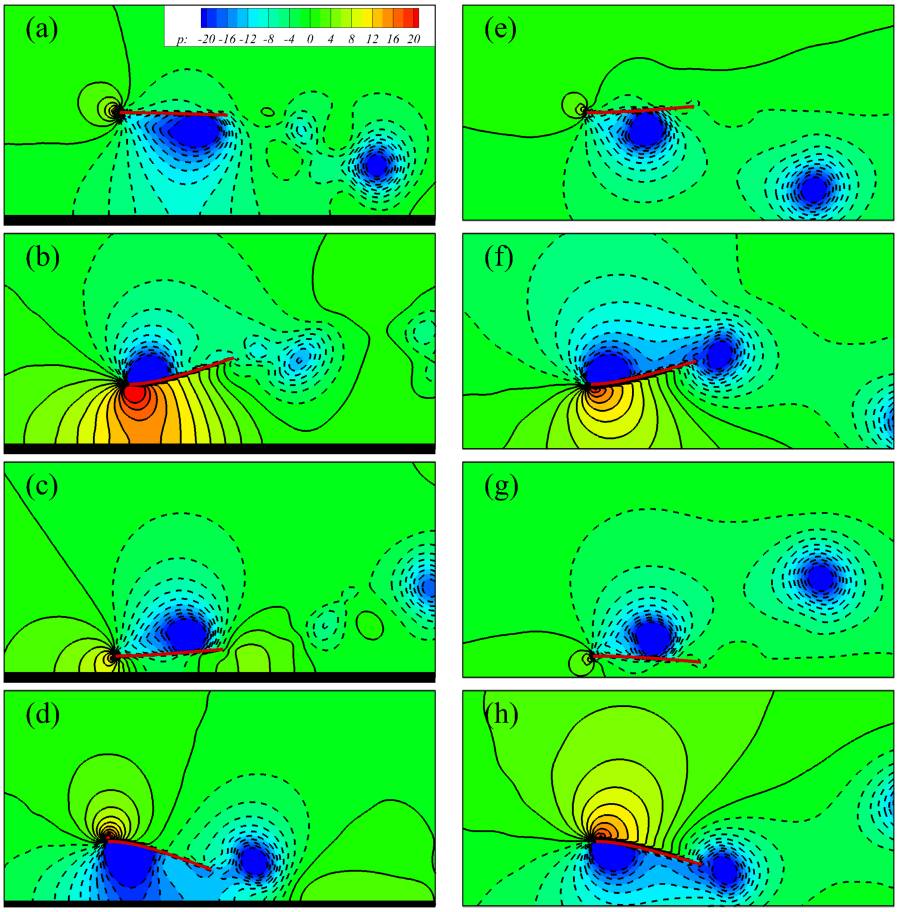

FIG. 13. Pressure contours at typical instants of one flapping cycle for Case 1A (left column) and Case 1B (right column) with $M = 0.3$: ((a) and (e)) $t/T = 0$, ((b) and (f)) 0.25, ((c) and (g)) 0.5, and ((d) and (h)) 0.75.

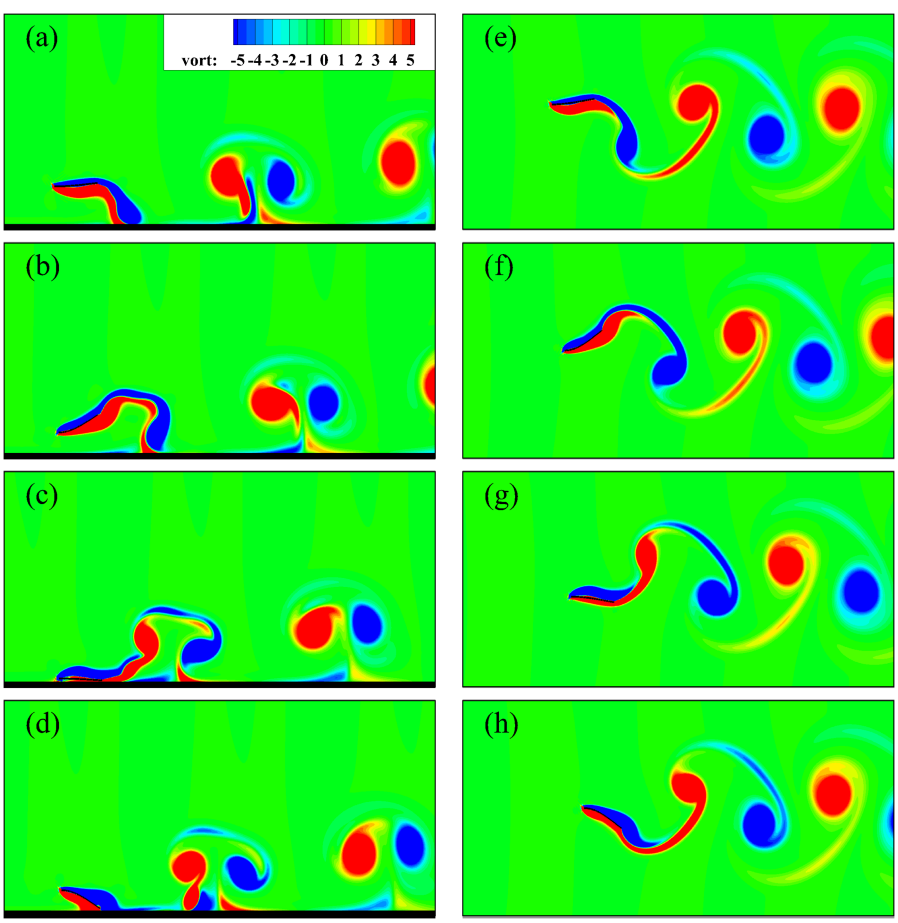

FIG. 14. Vorticity contours at typical instants of one flapping cycle for Case 2A (left column) and Case 2B (right column) with $A = 0.4$ and $M = 0.9$: ((a) and (e)) $t/T = 0$, ((b) and (f)) 0.25, ((c) and (g)) 0.5, and ((d) and (h)) 0.75.

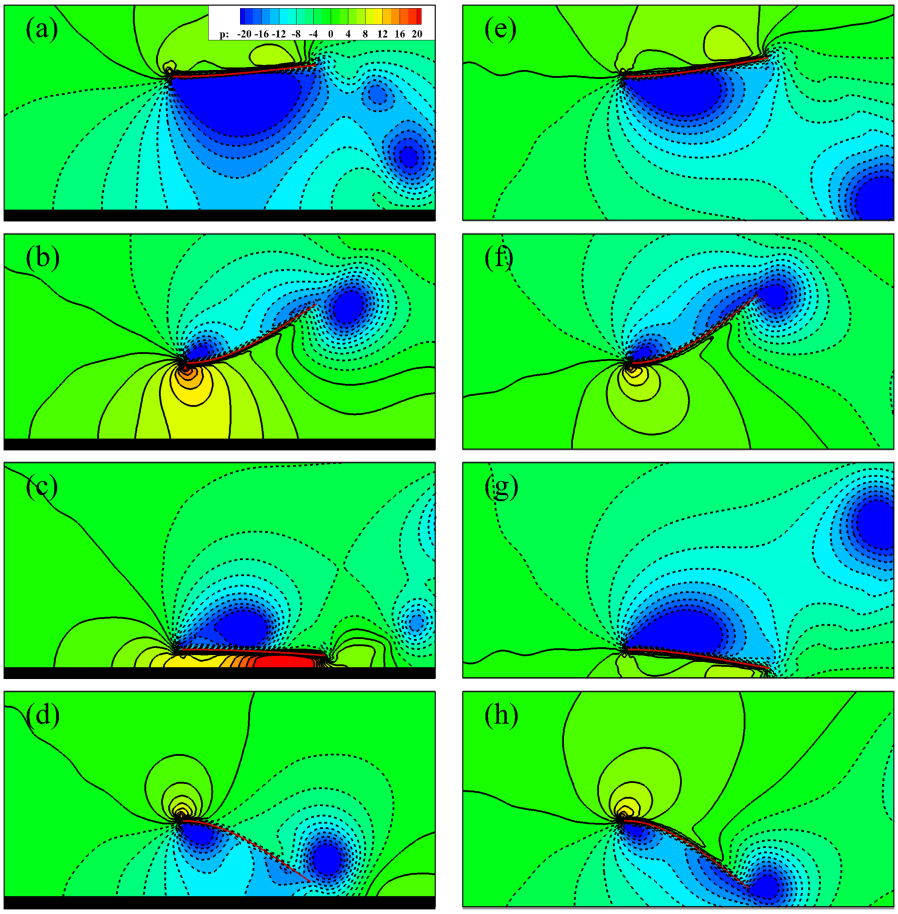

FIG. 15. Pressure contours at typical instants of one flapping cycle for Case 2A (left column) and Case 2B (right column) with $M = 0.9$: ((a) and (e)) $t/T = 0$, ((b) and (f)) 0.25, ((c) and (g)) 0.5, and ((d) and (h)) 0.75.

below the plate in Case 2A is lower than that in Case 2B, which prevents a large upward bending at the trailing edge in Case 2A. As the plate flaps downwards ($t/T = 0.25$), the lower leading part of the plate experiences a larger pressure shown in Figure 15(b) compared to Figure 15(f) due to a larger resistance that the plate encounters. At $t/T = 0.5$, the leading edge flaps to the location closest to the ground. The pressure between the plate and the ground in Figure 15(c) is much higher than that in Figure 15(g) especially near the tail of the plate which prevents the trailing-edge bending downwards too much. At $t/T = 0.75$, the pressure distributions in Figures 15(d) and 15(h) are similar. A very minor difference is that a lower pressure region near the trailing-edge in Figure 15(d) is closer to the middle upper surface of the plate than that in Figure 15(h), which induces a higher repulsive force near the tail. The higher repulsive force prevents the trailing edge of the plate bending downward. Correspondingly, the deformation in Case 2A is slightly inhibited compared to that in Case 2B.

From the discussion above, the pressure distribution around the plate, and therefore the deformation of the plate is changed due to the ground. The most significant point is that the pressure between the plate and ground is augmented by the inertia-dominated deformation. For example, the augment in Case 2A ($M = 0.9$) is larger than that in Case 1A ($M = 0.3$). Hence, $|C_L|$ is increased significantly in Case 2A than that in Case 1A.

From Eq. (10), the work done in the horizontal direction is zero. Only C_L and the deformation of the plate contribute to the work W. From discussions about the deformation and C_L, it is seen that for $M = 0.3$, $|C_L|$ is enhanced and the deformation is not sensitive to the distance in Case 1A, so the input work of Case 1A is larger than that of Case 1B due to the enhanced $|C_L|$. For $M = 0.9$, the inertial force dominates the hydrodynamic or aerodynamic behavior instead of the fluid force. Although $|C_L|$ in Case 2B is smaller than that in Case 2A (see Figure 15), the deformation of the plate in Case 2B is larger than that in Case 2A (see Figure 9). The overall input work W in one flapping cycle in Case 2B is still larger than that in Case 2A.

Hence, in principle the mechanism can be understood as follows: As we know, the input work is the product of force and velocity. For large M, as the plate approaches the ground, although $|C_L|$ is enhanced, the deformation of the plate is inhibited. The effect of inhibited deformation is more prominent, so the input work is reduced. By contrast, for small M, the deformation of the plate is not sensitive to the distance, and on the other hand the force ($|C_L|$) is enhanced as the plate approaches the plate, so the input work increases.

To study the effect of A on the wake structure, the instantaneous vorticity contours at the beginning instant of the downstroke is shown in Figure 16 for four typical cases. For the near-ground cases (the left column in Figure 16), D is fixed to be 0.7. As expected, when $A = 0.1$, the flapping amplitude is relatively small, and the ground effect is very minor. Hence, the wakes shown in Figures 16(a) and 16(b) are almost identical. In both cases, the shed vortices form a typical reverse von Karman vortex street. The propulsive properties of the two cases with $A = 0.1$ are almost identical (see Figure 7).

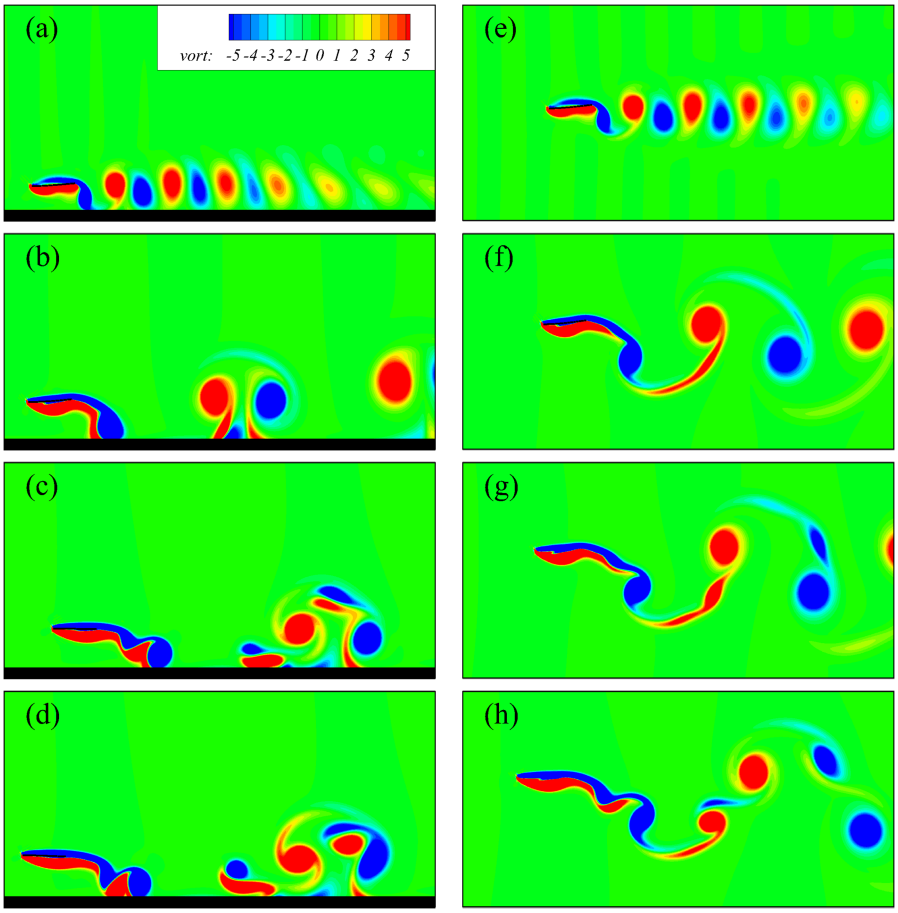

FIG. 16. Vorticity contours at the beginning instant of the downstroke ($t/T = 0$) for $D = 0.7$ (left column) and $D = \infty$ (right column) with $M = 0.5$: ((a) and (e)) $A = 0.1$, ((b) and (f)) 0.4, ((c) and (g)) 0.45, and ((d) and (h)) 0.5.

When $A = 0.4$, for the cases without the ground, the wake behind the plate is still a typical reverse von Karman vortex street, and the distance between the vortices increases (see Figure 16(d)). That means U increasing with A. Under the ground effect, small opposite vortices are induced on the ground (see Figure 16(c)), and two counter-rotating vortices in a vortex dipole shedding from the plate rotate as a whole. Hence, the vortices induced on the ground would roll up and shed from the ground to strengthen the original vortices shed from the plate. In this way, the ground enhances the propulsive performance of the plate.

When $A \geq 0.45$, for the cases without the ground, the wake behind the plate transits from "2S" pattern (Figure 16(f)) to "2P" pattern (see Figure 16(h)). Figures 16(c) and 16(d) show that for the near-ground cases, stronger vortices are produced on the ground, and there are vortex interactions between them. As mentioned in the end of Sec. IV A, there is an A_{cr} separating the "benefit-increase" and "benefit-decrease" regimes. The A_{cr} may be connected with the transition of the vortex shedding pattern.

V. CONCLUDING REMARKS

In order to study the ground effect on the self-propulsion of a flapping flexible plate, a series of numerical simulations were conducted. The problem is parameterized by a nondimensional ground distance, flapping amplitude, and density ratio of the plate and the fluid. Aerodynamic performance and the deformation of the plate due to the ground effect were investigated; we summarize the results of the study as follows.

First, for a specific bending rigidity K and flapping amplitude A, two appropriate density ratios are found to be able to optimize the propulsive efficiency and velocity, respectively. At a relatively small M, as the plate flapping near the ground, compared to the case without the ground, the input work W increases due to the increased repulsive force. At a larger M, as the plate flapping near the ground, the input work W decreases mainly due to the inhibited deformation of the plate.

Second, the ground effect does able to increase the propulsive speed and the propulsive efficiency. For a specific distance D, two distinct regimes which are separated by A_{cr} are identified, i.e., "benefit-increase" and "benefit-decrease" regimes. In the two regimes, the deformation of the plate is enhanced and inhibited, respectively. When $A > A_{cr}$, the propulsive efficiency reaches a plateau with the highest efficiency. A_{cr} may be directly connected with the transition of the vortex shedding pattern in cases without the ground.

Alternatively, the second point can be concluded as the following: When the flapping amplitude A is fixed, usually the closer the plate flapping is to the wall, the more efficient the propulsion is, provided that the tail of the plate would not touch the wall. On the other hand, when the plate flapping is close enough, with flapping amplitude $A > A_{cr}$, the efficiency may reache a plateau with the highest efficiency.

This study may shed some light on mechanism for self-propulsion of a flexible plate near the ground.

ACKNOWLEDGMENTS

This work was supported by the National Natural Science Foundation of China (Grant Nos. 11372304 and 11621202). Huang is also supported by the Fundamental Research Funds for the Central Universities.

[1]R. Blake, "The energetics of hovering in the mandarin fish (*Synchropus picturatus*)," J. Exp. Biol. **82**, 25 (1979).
[2]P. W. Webb, "The effect of solid and porous channel walls on steady swimming of steelhead trout *Oncorhynchus mykiss*," J. Exp. Biol. **178**, 97 (1993).
[3]F. R. Hainsworth, "Induced drag savings from ground effect and formation flight in brown pelicans," J. Exp. Biol. **135**, 431 (1988).
[4]D. B. Quinn, G. V. Lauder, and A. J. Smits, "Flexible propulsors in ground effect," Bioinspiration Biomimetics **9**, 036008 (2014).
[5]C. Tang, H. Huang, P. Gao, and X.-Y. Lu, "Self-propulsion of a flapping flexible plate near the ground," Phys. Rev. E **94**, 033113 (2016).
[6]S. Alben and M. Shelley, "Coherent locomotion as an attracting state for a free flapping body," Proc. Natl. Acad. Sci. U. S. A. **102**, 11163 (2005).
[7]S. E. Spagnolie, L. Moret, M. J. Shelley, and J. Zhang, "Surprising behaviors in flapping locomotion with passive pitching," Phys. Fluids **22**, 041903 (2010).
[8]T. Gao and X.-Y. Lu, "Insect normal hovering flight in ground effect," Phys. Fluids **20**, 087101 (2008).
[9]H. Lu, K. Lua, T. Lim, and K. Yeo, "Ground effect on the aerodynamics of a two-dimensional oscillating airfoil," Exp. Fluids **55**, 1787 (2014).
[10]J.-Y. Su, J.-H. Tang, C.-H. Wang, and J.-T. Yang, "A numerical investigation on the ground effect of a flapping-flying bird," Phys. Fluids **25**, 093101 (2013).
[11]A. Mivehchi, J. Dahl, and S. Licht, "Heaving and pitching oscillating foil propulsion in ground effect," J. Fluids Struct. **63**, 174 (2016).
[12]D. B. Quinn, K. W. Moored, P. A. Dewey, and A. J. Smits, "Unsteady propulsion near a solid boundary," J. Fluid Mech. **742**, 152 (2014).
[13]R. Wootton, R. Herbert, P. Young, and K. Evans, "Approaches to the structural modelling of insect wings," Philos. Trans. R. Soc., B **358**, 1577 (2003).
[14]S. Alben, C. Witt, T. V. Baker, E. Anderson, and G. V. Lauder, "Dynamics of freely swimming flexible foils," Phys. Fluids **24**, 051901 (2012).
[15]R.-N. Hua, L. Zhu, and X.-Y. Lu, "Locomotion of a flapping flexible plate," Phys. Fluids **25**, 121901 (2013).
[16]R. Fernández-Prats, V. Raspa, B. Thiria, F. Huera-Huarte, and R. Godoy-Diana, "Large-amplitude undulatory swimming near a wall," Bioinspiration Biomimetics **10**, 016003 (2015).
[17]J. Ryu, S. G. Park, B. Kim, and H. J. Sung, "Flapping dynamics of a flexible propulsor near ground," Acta Mech. Sin. **32**, 991 (2016).
[18]L. Dai, G. He, and X. Zhang, "Self-propelled swimming of a flexible plunging foil near a solid wall," Bioinspiration Biomimetics **11**, 046005 (2016).
[19]S. A. Combes and T. L. Daniel, "Into thin air: Contributions of aerodynamic and inertial-elastic forces to wing bending in the hawkmoth *Manduca sexta*," J. Exp. Biol. **206**, 2999 (2003).
[20]B. Yin and H. Luo, "Effect of wing inertia on hovering performance of flexible flapping wings," Phys. Fluids **22**, 111902 (2010).
[21]H. Dai, H. Luo, and J. F. Doyle, "Dynamic pitching of an elastic rectangular wing in hovering motion," J. Fluid Mech. **693**, 473 (2012).
[22]B. S. Connell and D. K. Yue, "Flapping dynamics of a flag in a uniform stream," J. Fluid Mech. **581**, 33 (2007).
[23]W.-X. Huang and H. J. Sung, "Three-dimensional simulation of a flapping flag in a uniform flow," J. Fluid Mech. **653**, 301 (2010).
[24]R.-N. Hua, L. Zhu, and X.-Y. Lu, "Dynamics of fluid flow over a circular flexible plate," J. Fluid Mech. **759**, 56 (2014).
[25]S. Chen and G. D. Doolen, "Lattice Boltzmann method for fluid flows," Annu. Rev. Fluid Mech. **30**, 329 (1998).
[26]C. S. Peskin, "The immersed boundary method," Acta Numer. **11**, 479 (2002).
[27]R. Mittal and G. Iaccarino, "Immersed boundary methods," Annu. Rev. Fluid Mech. **37**, 239 (2005).
[28]D. Goldstein, R. Handler, and L. Sirovich, "Modeling a no-slip flow boundary with an external force field," J. Comput. Phys. **105**, 354 (1993).
[29]W.-X. Huang, S. J. Shin, and H. J. Sung, "Simulation of flexible filaments in a uniform flow by the immersed boundary method," J. Comput. Phys. **226**, 2206 (2007).
[30]W.-X. Huang, C. B. Chang, and H. J. Sung, "An improved penalty immersed boundary method for fluid–flexible body interaction," J. Comput. Phys. **230**, 5061 (2011).
[31]F.-B. Tian, H. Luo, L. Zhu, J. C. Liao, and X.-Y. Lu, "An efficient immersed boundary-lattice Boltzmann method for the hydrodynamic interaction of elastic filaments," J. Comput. Phys. **230**, 7266 (2011).
[32]J. Doyle and E. DeSantiago, "Nonlinear analysis of thin-walled structures: Statics, dynamics, and stability. Mechanical engineering series," Appl. Mech. Rev. **55**, B92 (2002).
[33]C. Tang, N.-S. Liu, and X.-Y. Lu, "Dynamics of an inverted flexible plate in a uniform flow," Phys. Fluids **27**, 073601 (2015).
[34]G.-J. Li and X.-Y. Lu, "Force and power of flapping plates in a fluid," J. Fluid Mech. **712**, 598 (2012).
[35]J. Zhang, N.-S. Liu, and X.-Y. Lu, "Locomotion of a passively flapping flat plate," J. Fluid Mech. **659**, 43 (2010).
[36]R. Bainbridge, "The speed of swimming of fish as related to size and to the frequency and amplitude of the tail beat," J. Exp. Biol. **35**, 109 (1958).
[37]C. P. Ellington, "The aerodynamics of hovering insect flight. II. Morphological parameters," Philos. Trans. R. Soc., B **305**, 17 (1984).
[38]C. Ellington, "The aerodynamics of hovering insect flight. III. Kinematics," Philos. Trans. R. Soc., B **305**, 41 (1984).
[39]F. E. Fish, "Power output and propulsive efficiency of swimming bottlenose dolphins (*Tursiops truncatus*)," J. Exp. Biol. **185**, 179 (1993).
[40]G. K. Taylor, R. L. Nudds, and A. L. Thomas, "Flying and swimming animals cruise at a Strouhal number tuned for high power efficiency," Nature **425**, 707 (2003).
[41]J.-S. Chen, J.-Y. Chen, and Y.-F. Chou, "On the natural frequencies and mode shapes of dragonfly wings," J. Sound Vib. **313**, 643 (2008).
[42]S. Jongerius and D. Lentink, "Structural analysis of a dragonfly wing," Exp. Mech. **50**, 1323 (2010).
[43]B. Thiria and R. Godoy-Diana, "How wing compliance drives the efficiency of self-propelled flapping flyers," Phys. Rev. E **82**, 015303 (2010).
[44]S. Kern and P. Koumoutsakos, "Simulations of optimized anguilliform swimming," J. Exp. Biol. **209**, 4841 (2006).